

Photovoltaic efficiency of transition metal dichalcogenides thin films by *ab initio* excited-state methods

Enesio Marinho Jr,^{*,†} Cesar E. P. Villegas,^{*,¶} Pedro Paulo de Mello Venezuela,^{*,§}
and Alexandre Reily Rocha^{*,‡}

[†] *Departamento de Física e Química, Universidade Estadual Paulista (UNESP),
Av. Brasil, 56, Ilha Solteira, 15385-007 São Paulo, Brazil.*

[‡] *Instituto de Física Teórica, Universidade Estadual Paulista (UNESP),
R. Dr. Bento Teobaldo Ferraz, 271, São Paulo, 01140-070 São Paulo, Brazil.*

[¶] *Departamento de Ciencias, Universidad Privada del Norte, Lima 15434, Peru
§Instituto de Física, Universidade Federal Fluminense (UFF),*

Av. Gal. Milton Tavares de Souza, s/n, 24210-346 Niterói, Rio de Janeiro, Brazil.

E-mail: enesio.marinho@unesp.br; cesar.villegas@unesp.br; pedrovenezuela@id.uff.br;
alexandre.reily@unesp.br

Abstract

Transition metal dichalcogenides (TMDCs) have garnered significant interest in optoelectronics, owing to their scalability and thickness-dependent electrical and optical properties. In particular, thin films of TMDCs could be used in photovoltaic devices. In this work, we employ *ab initio* many-body perturbation theory within G_0W_0 -BSE approach to accurately compute the optoelectronic properties of thin films of 2H-TMDCs composed of Mo, W, S, and Se. Subsequently, we evaluate their photovoltaic performance including exciton recombination effects, and show this is a key ingredient. We

obtain efficiencies of up to 29% for a 200-nm thick film of WSe₂, thus providing an upper limit. We also include other phenomenological recombination mechanisms that could be present in current samples. This slightly reduces efficiencies, indicating that even with current synthesis technologies, there is still potential for further enhancement of TMDCs' performance in photovoltaic applications.

Keywords: Transition metal dichalcogenides · Photovoltaic efficiency · Optoelectronics · Thin films · MBPT · *GW*-BSE

Introduction

Layered van der Waals (vdW) materials consist of stacked two-dimensional (2D) sheets interacting via dispersion forces. Graphite is a well-known member of this family that is broadly used in industry as components for electrodes, lubricants, fibers, heat exchangers, and batteries.¹ The experimental isolation of its single-layer counterpart, graphene² has opened the way for a new era of 2D materials with compelling optoelectronic properties.³⁻⁵ However, the lack of an energy gap in graphene greatly limits its applicability in semiconductor technologies. On the other hand, the semiconducting properties of transition metal dichalcogenides (TMDCs), with chemical formula MX₂ (M = Mo, W, and others, and X = S, Se, Te) pushed the frontier of vdW materials' potential uses spanning a broad range of fields, including nanoelectronics and nanophotonics, sensing and actuation in the nanoscale, and photovoltaic solar cells.⁶⁻¹²

The TMDCs monolayers present direct bandgaps ranging from ~ 1.4 to 2.5 eV,¹³ which is well-suited for solar energy absorption,¹⁴ particularly as ultra-thin photon absorbers for applications in transparent and flexible solar cells.^{15,16} Theoretical predictions indicate that the TMDCs monolayers should present absorption coefficients per unit thickness one to two orders of magnitude greater than those of conventional semiconductors.¹⁷ This is achieved due to the localized nature of electronic wave functions, leading to van Hove singularities in

the density of states. These strong peaks are accountable for the heightened photoresponsivity observed in these 2D materials.¹⁸ As a consequence, with a thickness of less than 1 nm, in principle, they can absorb an amount of visible light comparable to 15 nm of GaAs or 50 nm of Si,¹⁷ which makes them a promising choice for efficient photovoltaic applications. However, in practice, the power conversion efficiency (PCE) of single layer TMDC solar cells has typically not exceeded 2%.^{19–24} This is mostly due to strong Fermi-level pinning at the metal–semiconductor interface,²⁵ and high probability of carrier recombination caused by defective surfaces, which leads to a low open-circuit voltage (V_{oc}).¹⁵

In order to overcome those performance issues, some TMDC-based solar cells have been assembled by using few-layered or multi-layered stacks of 2H-TMDCs. Lee et al.²⁶ have studied the photovoltaic response of graphene-sandwiched MoS₂/WSe₂ heterostructures with different thicknesses. They reported a high short-circuit current density of ~ 2.2 A/cm², measured under laser light ($\lambda = 532$ nm). For comparison, the authors also reported the short-circuit current of vertical heterojunctions composed of single atomic layers of MoS₂ (n -doped) and WSe₂ (either p -doped or ambipolar) with a value of ~ 1 mA/cm². The external quantum efficiency (EQE) is also dependent on the number of layers. The measured EQEs at 532 nm were 2.4%, 12%, and 34% for monolayer, bilayer, and multilayer p–n junctions. Memaran et al.²⁷ have studied the photovoltaic efficiency of the MoSe₂ crystal composed of ~ 10 atomic layers transferred onto a flat hBN crystal creating an electrostatic p–n junction. They have reported photovoltaic efficiencies surpassing 14% under AM-1.5 spectrum, with concomitant fill factors approaching 0.7.

More recently, Cho et al.²⁸ proposed a transparent thin-film photovoltaic cell composed by a heterojunction of WSe₂/MoS₂ and an indium tin oxide electrode. Their device is highly transparent ($\sim 80\%$) and presents a PCE of $\sim 10\%$. Also, high-specific-power flexible transition metal dichalcogenide solar cells have been fabricated by employing transparent graphene contacts and MoO_{*x*} capping for doping, passivation, and anti-reflection.²⁹ These lead to PCE of 5.1% and specific power of 4.4 Wg^{−1} for flexible WSe₂ solar cells.

These observations suggest that junctions composed of few-layered or multilayered TMDCs can yield higher photovoltaic responses compared to monolayers. Nonetheless, while monolayer TMDCs have been extensively studied and well characterized for photovoltaic applications, their bulk counterparts were less so, especially from a microscopic point of view. In this sense, a highly accurate and reliable *ab initio* prediction of the optoelectronic properties and photovoltaic efficiencies of bulk 2H-TMDCs is crucial.

Herein, we employ *ab initio* many-body perturbation theory within the *GW*-BSE scheme to investigate the optoelectronic properties of bulk 2H-TMDCs and then address their theoretical photovoltaic efficiencies. We analyze the power-conversion efficiency of MX_2 TMDCs with $\text{M} = \text{Mo}, \text{W}$ and $\text{X} = \text{S}, \text{Se}$, modeling the inclusion of nonradiative recombination losses with exciton eigenvalues computed by BSE, in an approach we denote as SLME-X which has already been proposed by Ozório and co-workers,³⁰ and compared those results with another modeling in which we estimate the fraction of radiative recombination processes using reported values obtained by photoluminescence quantum yield experiments (SLME-PLQY). Applying the SLME-X approach, the photovoltaic efficiencies of the TMDCs consistently fell within the range of 23% to 29%, reaching efficiencies analogous to those obtained using the Shockley-Queisser formalism. On the other hand, when we employ the SLME-PLQY framework, the power conversion efficiencies tend to be reduced, ranging from 19% to 24%.

Computational Methods

Ground-state atomic structures were obtained by first-principles calculations based on density-functional theory (DFT)^{31,32} as implemented in the Quantum ESPRESSO package.³³ The Perdew-Burke-Ernzerhof generalized-gradient approximation³⁴ was employed to describe the exchange-correlation functional. Fully relativistic optimized norm-conserving Vanderbilt pseudopotentials (ONCVSP),³⁵ considering semicore s and p states as valence electrons, are used to describe the electron-ion interaction. A kinetic energy cutoff of 84 Ry

is set to expand the Kohn-Sham orbitals. The charge density is obtained in a Γ -centered Monkhorst-Pack k -point sampling of $8 \times 8 \times 4$. The structures are fully relaxed including van der Waals corrections within the semi-empirical dispersion scheme (PBE-D2) as proposed by Grimme,³⁶ and also including spin-orbit coupling.

The many-body perturbation theory (MBPT) framework within the GW approximation³⁷ has been applied to compute the quasiparticle energies of bulk 2H-TMDCs by using the YAMBO code.³⁸ The dielectric screening $\epsilon_{\mathbf{G},\mathbf{G}'}(\mathbf{q},\omega)$ is obtained considering the Plasmon-Pole approximation in a \mathbf{k} -grid of $12 \times 12 \times 4$, with an energy cutoff of 60 Ry for the exchange potential and 30 Ry for the screened interaction W_0 . Both the Green's functions and the screened Coulomb interaction are calculated including 600 bands. This number of bands is sufficient to provide accurate results thanks to the implementation of the Bruneval-Gonze terminators approach.³⁹

The electron-hole (e-h) interaction is included in the calculation of the optical absorption spectra of the 2H-TMDCs by means of the Bethe-Salpeter equation (BSE), which can be written adopting the Tamm-Dancoff approximation as an effective eigenvalue problem

$$\sum_{v'c'\mathbf{k}'} H_{v\mathbf{c}\mathbf{k}}^{\text{BSE}} A_{v'c'\mathbf{k}'}^S = \Omega_S A_{v\mathbf{c}\mathbf{k}}^S, \quad (1)$$

where $A_{v\mathbf{c}\mathbf{k}}^S$ and Ω_S are the exciton eigenfunction and the eigenvalues for the S -th exciton, respectively. In this form, the BSE Hamiltonian is given by

$$H_{v\mathbf{c}\mathbf{k}}^{\text{BSE}} = \left(\epsilon_{c\mathbf{k}}^{\text{QP}} - \epsilon_{v\mathbf{k}}^{\text{QP}} \right) \delta_{c,c'} \delta_{v,v'} \delta_{\mathbf{k},\mathbf{k}'} + \Xi_{v\mathbf{c}\mathbf{k},v'c'\mathbf{k}'}, \quad (2)$$

where the first term comprises a diagonal part that contains the quasiparticle energy differences, and $\Xi = \bar{v} - W$ is the e-h interaction kernel, composed of a bare, repulsive short-range exchange term, and an attractive static screened Coulomb potential.⁴⁰

To speed up the BSE calculations, we employ the double-grid method⁴¹ in which the kernel matrix elements are calculated on a coarse \mathbf{k} -grid (the same used for the GW calcu-

lations), and then interpolated on a finer \mathbf{k} -grid sampling of $60 \times 60 \times 8$, including eight valence bands and eight conduction bands. These values are sufficient to obtain converged results for the lowest peaks of the optical absorption. A full analysis of the convergence of all the relevant parameters related to GW and BSE calculations is presented in the Supporting Information.⁴²

The optical absorption is calculated considering the imaginary part of the dielectric function

$$\epsilon_2(\omega) = \frac{4\pi^2}{VN_k} \sum_S \left| \sum_{v\mathbf{c}\mathbf{k}} A_{v\mathbf{c}\mathbf{k}}^S \hat{\mathbf{e}} \cdot \langle v\mathbf{k} | \mathbf{r} | c\mathbf{k} \rangle \right|^2 \delta(\omega - \Omega_S), \quad (3)$$

where V is the volume, N_k is the number of points in the Brillouin zone sampling, $\hat{\mathbf{e}}$ is the light polarization vector, and $\langle v\mathbf{k} | \mathbf{r} | c\mathbf{k} \rangle$ are the single-particle dipole matrix elements.

Results and Discussion

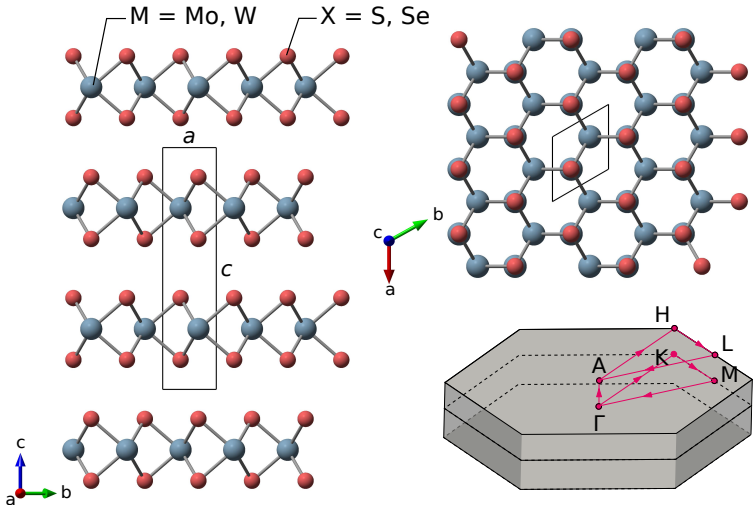


Figure 1: Top and side views of the crystal structure of bulk transition metal dichalcogenides MX_2 in trigonal prismatic (2H) phase, where M (blue) is the transition metal Mo or W, and X (red) is the chalcogen atom S or Se. The first Brillouin zone is also represented with high-symmetry \mathbf{k} -points and paths.

The computed fully-relaxed crystal structure is shown in Fig. 1, and the lattice parameters

Table 1: Fully-relaxed lattice parameters for bulk 2H-TMDCs considering PBE-D2 van der Waals corrections and fully including spin-orbit coupling. The respective experimental values from Refs. ^{43–45} are shown for comparison.

	MoS ₂	MoSe ₂	WS ₂	WSe ₂
PBE-D2-SOC				
a (Å)	3.19	3.32	3.19	3.34
c (Å)	12.42	13.03	12.16	12.81
Experiment				
a (Å)	3.16 ^a	3.29 ^b	3.15 ^c	3.28 ^c
c (Å)	12.29 ^a	12.93 ^b	12.32 ^c	12.96 ^c

^a Ref.;⁴³ ^b Ref.;⁴⁵ ^c Ref.⁴⁴

of the studied bulk systems are summarized in Table 1, which are in good agreement with experimental results. ^{43–45}

Subsequently, we compute the quasiparticle band structures and band gaps of the bulk TMDCs using the G_0W_0 approximation including spin-orbit coupling. The results are presented in Fig. 2 and Table 2. Our results, which include both direct and indirect quasiparticle band gap values, align well with the previously reported G_0W_0 findings. ¹³ Moreover, our calculations are in agreement with the band gaps and spin-splitting observed for the valence band, denoted as Δ_V , as measured through ARPES according to Kim et al. ⁴⁶ It can be seen that the band gaps of the TMDCs are similar for those systems with the same chalcogen species.

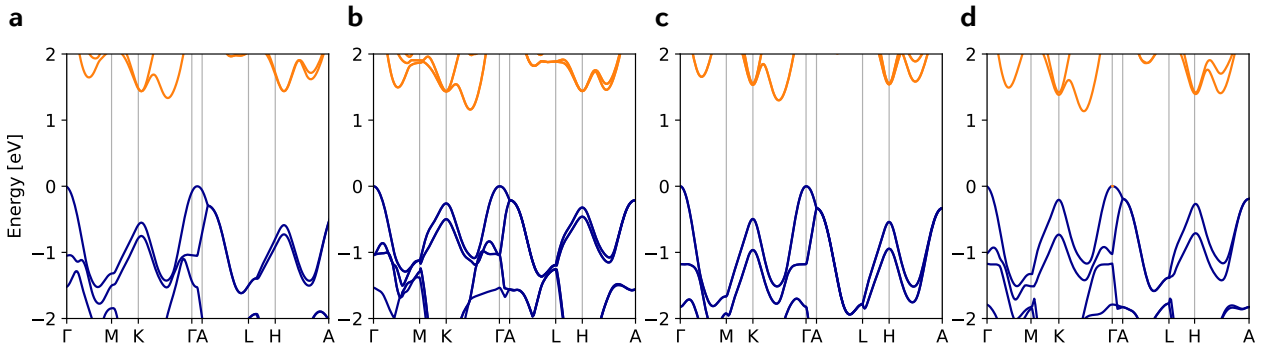


Figure 2: Quasiparticle band structure of (a) MoS₂, (b) MoSe₂, (c) WS₂ and (d) WSe₂ within G_0W_0 approximation including spin-orbit coupling.

Table 2: Quasiparticle fundamental (indirect) and direct band gap (in eV) at K point in the Brillouin zone, calculated within G_0W_0 approximation; spin-splitting for the valence band Δ_V (in meV); ground-state and A excitonic peak energy positions (X_{gs} , X_A), and Boltzmann factor Δ_X for the fraction of the radiative e-h recombination in the SLME-X approach for the bulk 2H-TMDCs (see text for further details). For comparison, we present the band gaps and spin-splitting Δ_V obtained by ARPES.⁴⁶

	E_g^i	E_g^d	Δ_V	X_{gs}	X_A	Δ_X
MoS ₂	1.34	1.99	0.20	1.846	1.877	0.031
	1.14 ^a	1.82 ^a	0.16 ^a			
MoSe ₂	1.16	1.69	0.24	1.583	1.607	0.024
	1.25 ^a	1.57 ^a	0.20 ^a			
WS ₂	1.30	2.02	0.47	1.915	1.956	0.041
	1.25 ^a	1.82 ^a	0.44 ^a			
WSe ₂	1.14	1.59	0.49	1.511	1.561	0.050
	1.12 ^a	1.62 ^a	0.48 ^a			

^a Ref.⁴⁶

Turning to the optical properties, the computed imaginary part of the dielectric function at both the independent particle (IP) level and including e-h interaction are shown in Fig. 3. For comparison, we also show the experimental optical absorption results (Refs.⁴⁷ and⁴⁸) for the respective TMDCs (shadow areas).

We notice a good agreement between the BSE optical spectra and the experimental ones, highlighting the excitons' role in the optical absorption of bulk TMDCs. Overall, our findings effectively capture the essential characteristics of the experimental spectra, albeit with slightly diminished accuracy for W-based TMDCs primarily attributable to the increased splitting of electronic bands induced by higher spin-orbit coupling. The lack of prominent peaks in the IP spectrum strongly suggests that the sharp redshifted X peaks observed in BSE are associated with excitonic features. The absorption spectra calculated within IP exhibit noticeably weaker and less defined shoulder-like characteristics, indicating primarily band transitions. The two lowest energy peaks correspond to the excitonic states labeled as A and B, which are associated with interband transitions at the K point in the Brillouin

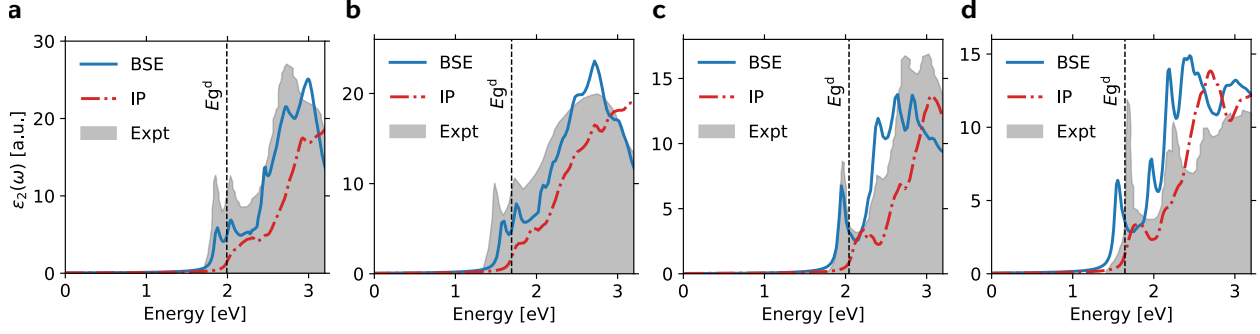


Figure 3: Optical spectra calculated at the BSE (blue solid line) and independent particle (IP, red dot-dashed line) levels for the bulk (a) MoS₂, (b) MoSe₂, (c) WS₂, and (d) WSe₂. The Kohn-Sham eigenvalues include the quasiparticle corrections of the G_0W_0 calculations. The experimental data (gray shadow areas) are taken from Refs. ^{47,48}

zone, coming from the splitting of the valence band due to spin-orbit coupling. ^{49,50}

Our results indicate that the ground-state exciton (X_{gs}) for all the studied systems corresponds to a dark state, that rises from transitions between the valence band maximum and conduction band minimum at the K point. The corresponding excitonic peak energy position of X_{gs} and X_A for the TMDCs are summarized in Table 2.

Now we investigate the photovoltaic efficiency of the bulk TMDCs. Yu and Zunger ⁵¹ developed the so-called spectroscopic limited maximum efficiency (SLME) model to compute the maximum efficiency of the absorber in a single-junction solar cell. In this formalism, the magnitude of the fundamental band gap, the values of the direct and indirect electronic gaps, the standard solar spectrum, the absorption coefficient of the material, and the thickness are taken into account to estimate the PCE of the device

$$\eta_{\text{SLME}} = \frac{P_m}{P_{\text{in}}}, \quad (4)$$

where P_{in} is the total incident power density with a value of 1000.37 W/m², and P_m is the maximum output power density which can be obtained by maximizing the product of current density, J , and voltage, V ,

$$P = JV = \left[J_{\text{sc}} - J_0(e^{eV/k_B T} - 1) \right] V, \quad (5)$$

where k_B is the Boltzmann constant, and T is the device temperature taken as $T = 298.15$ K throughout this work. Both the short circuit current density J_{sc} and the reverse saturation current density J_0 are calculated from the photon absorptivity $a(\omega)$ of the material as follows

$$a(\omega) = 1 - e^{-2\alpha(\omega)L}, \quad (6)$$

where $\alpha(\omega)$ is the absorption coefficient computed from first principles, and L is the thickness of the photovoltaic absorber material taken as 500 nm unless otherwise stated. In this regard, those current densities can be described including the AM1.5G solar spectrum $I_{\text{sun}}(\omega)$ and the black-body spectrum $I_{\text{bb}}(\omega, T)$, respectively

$$J_{sc} = e \int_{E_g}^{\infty} a(\omega) I_{\text{sun}}(\omega) d\omega, \quad (7)$$

$$J_0 = \frac{J_0^r}{f_r} = \frac{e\pi}{f_r} \int_{E_g}^{\infty} a(\omega) I_{\text{bb}}(\omega, T) d\omega. \quad (8)$$

J_0 corresponds to the total e-h recombination current at equilibrium in the dark, regarding both radiative and non-radiative recombinations. Here, f_r is proposed as the fraction of the radiative recombination current, which in the original SLME framework is modeled using a Boltzmann factor

$$f_r = e^{-\Delta_r/k_B T}, \quad (9)$$

where $\Delta_r \equiv E_g^{\text{da}} - E_g$ is the difference between the allowed direct band gap and the fundamental band gap, respectively.

Note that the efficiency within the Shockley–Queisser (SQ) detailed balance limit⁵² (η_{SQ}) can be obtained from the equations above by setting $f_r = 1$ and considering the absorbance in Eq. (7) and (8) as a Heaviside step function that vanishes for $E < E_g$ and is equal to 1 for $E \geq E_g$, where E_g is the optical band gap of the photovoltaic absorber.

It is important to notice that for indirect band gap materials with large Δ_r , as in the

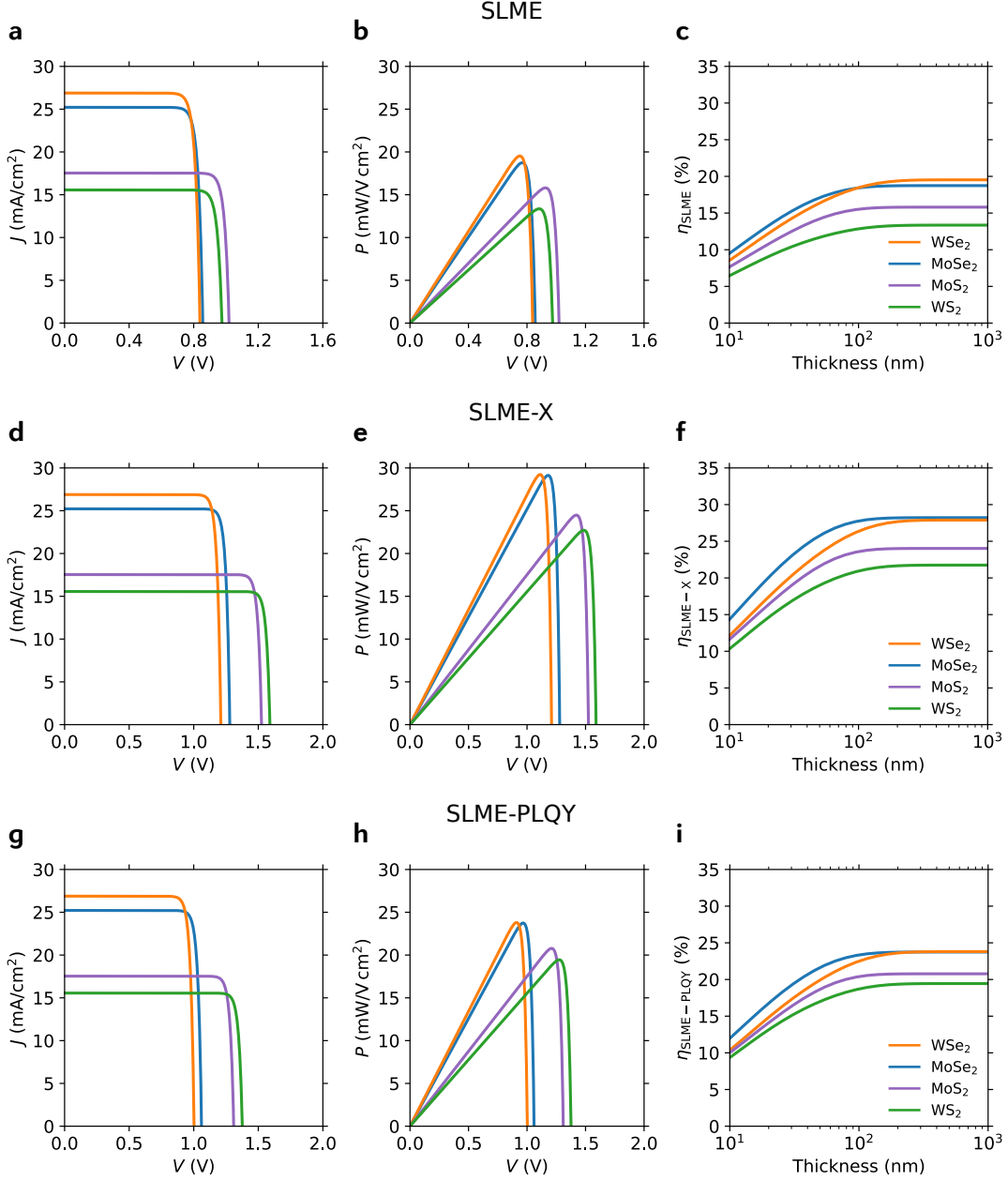


Figure 4: Photovoltaic properties of bulk 2H-TMDCs calculated using the spectroscopic limited maximum efficiency (SLME) framework (a-c), modeling the fraction of radiative recombination losses (f_r) by considering the exciton eigenvalues from BSE (SLME-X) (d-f), and by extracting the fraction of the radiative losses directly from photoluminescence quantum yield experiments⁵³ (SLME-PLQY) (g-i): J - V , P - V curves, and power conversion efficiency (η) as a function of the thickness of the absorber. The results have been computed for a device temperature of $T = 298.15$ K.

TMDCs studied here, the original SLME approach can drastically underestimate the predicted PCE, given that the Boltzmann factor rapidly decreases the fraction of radiative

Table 3: Photovoltaic properties of bulk TMDCs obtained within the Shockley-Queisser approach and the spectroscopic limited maximum efficiency (SLME) standard framework, by modeling the fraction of radiative recombination losses (f_r) by considering the exciton eigenvalues from BSE (SLME-X), and by extracting the fraction of the radiative losses directly from photoluminescence quantum yield experiments⁵³ (SLME-PLQY): short-circuit current densities (J_{sc}), open-circuit voltage (V_{oc}), fill factor (FF), and power-conversion efficiency (η).

	Shockley-Queisser				SLME			
	J_{sc} (mA/cm ²)	V_{oc} (V)	FF (%)	η_{SQ} (%)	J_{sc} (mA/cm ²)	V_{oc} (V)	FF (%)	η_{SLME} (%)
MoS ₂	17.5	1.55	92.2	25.0	17.5	1.02	88.6	15.8
MoSe ₂	25.2	1.30	90.7	29.7	25.2	0.86	86.5	18.7
WS ₂	15.6	1.63	91.8	23.3	15.6	0.98	87.4	13.4
WSe ₂	26.9	1.26	90.1	30.5	26.9	0.84	86.4	19.5

	SLME-X				SLME-PLQY			
	J_{sc} (mA/cm ²)	V_{oc} (V)	FF (%)	η_{SLME-X} (%)	J_{sc} (mA/cm ²)	V_{oc} (V)	FF (%)	$\eta_{SLME-PLQY}$ (%)
MoS ₂	17.5	1.52	92.0	24.5	17.5	1.31	90.5	20.8
MoSe ₂	25.2	1.28	90.3	29.1	25.2	1.06	88.8	23.7
WS ₂	15.6	1.59	91.6	22.7	15.6	1.37	91.1	19.4
WSe ₂	26.9	1.21	89.8	29.2	26.9	1.01	88.1	23.8

recombination current density f_r . Consequently, the saturation current J_0 is overestimated, yielding lower values for the open-circuit voltages. This effect was studied in detail by Bercx *et al.*⁵⁴ for silicon, which possesses a $\Delta_r = 2.23$ eV. This leads to a PCE of zero regardless of the temperature and thickness of the material.

First, we apply the standard SLME formalism to compute the PCEs considering Δ_r as the difference between X_A and E_g^i . Employing this approach, for all the analyzed systems, the fraction of radiative recombination current, f_r , is much smaller than 10^{-8} , leading to PCEs varying between 13% and 19% for the studied TMDCs, significantly smaller than those obtained through Shockley-Queisser (Table 3). This result suggests that, for these materials, employing the original SLME approach implies that almost all e-h recombination would be non-radiative, even though J_0 is modeled assuming a black-body spectrum, which relies on a radiative principle. This issue motivated us to explore alternative models for describing the recombination factor.

Delving into this possibility, and taking into account that the excitonic effects in bulk

TMDCs play a key role in their optical responses, we also compute the PCE using a slightly modified SLME approach that has been proposed by Ozório and co-workers.³⁰ In their model, the fraction of the radiative recombination current, f_r , is calculated by replacing the Δ_r in Eq. (9) with Δ_X , which is defined as

$$\Delta_X = X_A - X_{gs}. \quad (10)$$

We refer to this approach as exciton-based SLME or SLME-X. Within it, the fraction of the radiative recombination current, f_r , calculated taking into account the Δ_X values presented in Table 2. As a result, the obtained f_r values vary between 1.5×10^{-2} and 3.9×10^{-2} . It is important to point out that the presence of an indirect gap could lead to lower energy dark excitons that lead to non-radiative decay. Thus, the most effective method for obtaining the exciton ground state involves computing the q -dependent BSE spectra.⁵⁵ In that case, we expect that f_r would have even lower values, although still surpassing those obtained within the standard SLME.

In Fig. 4a-b, we show the current and power density curves as a function of the voltage, obtained with the SLME-X approach. The PCE as a function of thickness is depicted in Fig. 4c. All the main solar cell parameters obtained from these curves are summarized in Table 3.

We can verify that all the investigated photovoltaic properties are similar for those TMDCs that are composed of the same chalcogen species. The transition metal diselenides should have higher photovoltaic efficiencies than disulfides due to their lower optical band gaps. In addition, our results presented in Fig. 4(c) indicate that $\eta_{\text{SLME-X}}$ saturates for a thickness around 10^2 nm.

Alternatively, non-radiative recombination losses can be experimentally quantified by the photoluminescence quantum yield (PLQY).⁵⁶ We can also estimate the maximum PCE by assuming that the PLQY is, in principle, equal to the fraction of radiative recombination

(f_r).⁵⁷ We denote this other modified SLME approach as SLME-PLQY. Experimental studies have reported that for single-layer TMDCs, the PLQY is close to unity.^{53,58,59} In contrast, it has been demonstrated that the PLQY for their bulk counterpart is reduced by a factor of 10^4 .⁶⁰

We adopt the PLQY values reported by Mohamed and co-workers⁵³ as the experimental-based f_r for the TMDCs. These f_r values are 6.8×10^{-5} , 7.9×10^{-5} , 4.9×10^{-5} , and 4.5×10^{-5} for the bulk MoS₂, MoSe₂, WS₂ and WSe₂, respectively.

Considering the SLME-PLQY approach, we also calculate the current density-voltage, power density-voltage, and PCE-thickness curves of the studied TMDCs, which are shown in Fig. 4d-f. For comparison with the SLME-X results, we describe the solar cell parameters obtained within SLME-PLQY for the TMDCs in Table 3. Given that the short-circuit current densities, J_{sc} , do not depend on the fraction of the radiative recombination current, their values are identical for both approaches. On the other hand, the open-circuit voltages and fill factors are smaller in the SLME-PLQY approach in comparison to the SLME-X one, leading to smaller values of PCE in the latter case.

All the obtained results of the photovoltaic efficiencies within the SQ and SLME-based approaches are summarized in Fig. 5, where we present the maximum PCE as a function of the optical band gap. For the analyzed TMDCs, the average of the fraction of e-h radiative recombination is $f_r = 3 \times 10^{-8}$ for the standard SLME, $f_r = 6 \times 10^{-5}$ for SLME-PLQY and $f_r = 3 \times 10^{-2}$ for SLME-X. In addition, we have estimated the error associated with those average maximum PCEs, by introducing in the f_r the error threshold of the *GW* calculations (see Fig. S5 in the Supporting Information). As a result, regarding the SLME approach, for systems with optical gaps close to 1.9 eV (MoS₂, WS₂), the estimated error is $\sim 1\%$, whereas for those with optical gaps around 1.6 eV (MoSe₂, WSe₂), the error can be approximately 2.4%. Considering this uncertainty estimate, we expect comparable errors for the remaining formalisms.

Based on these fractions of non-radiative e-h recombination, we compute the efficiencies

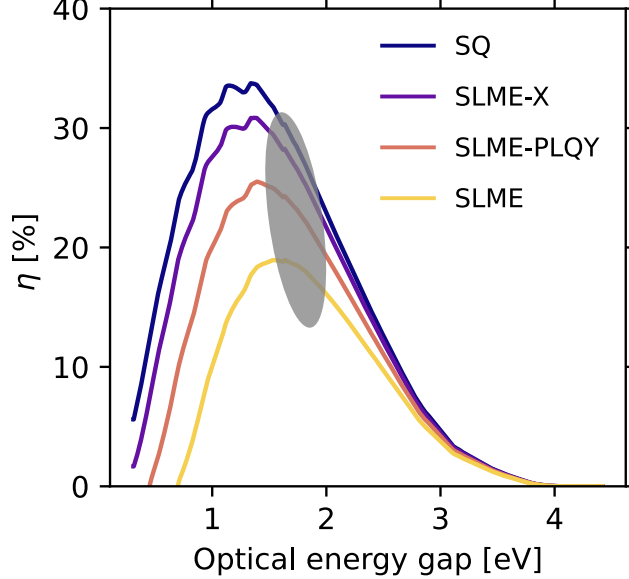


Figure 5: Power conversion efficiency with respect to the optical energy gap in Shockley-Queisser and SLME-based approaches. The plotted curves, derived from the average computed fraction of e-h radiative recombination (f_r) for the studied TMDCs, illustrate the impact of nonradiative recombination losses in the PCE. Alongside the standard SLME, we incorporate considerations from exciton eigenvalues obtained through BSE (SLME-X) and direct estimations from photoluminescence quantum yield analyses experiments (SLME-PLQY). The shaded area denotes the range of optical band gaps associated with the analyzed TMDCs.

as a function of the optical energy gap. The shaded area in Fig. 5 represents the range of optical band gaps corresponding to the TMDCs studied. We can verify that the SQ formalism, which considers only radiative recombination processes ($f_r = 1$), overestimates the photovoltaic efficiency of the bulk TMDCs, with photovoltaic efficiencies ranging from $\sim 23\%$ to $\sim 29\%$ (Table S1 in the Supporting Information⁴²). On the other hand, all the SLME-based approaches include a non-vanishing fraction of non-radiative e-h recombination ($f_r < 1$), decreasing the predicted photovoltaic efficiencies of the absorbers.

Our results suggest that even the highest quality TMDC-based thin film would yield maximum efficiencies between $\sim 23 - 29\%$, if we take into account only excitonic effects as a fundamental factor to describe the recombination processes. Nevertheless, a more realistic upper limit of the photovoltaic efficiency for the investigated TMDCs can be predicted by considering the fraction of the radiative recombination directly from PLQY experiments,

with the TMDC thin-films reaching maximum PCEs between $\sim 19 - 21\%$. Based on it, it is noticeable that PLQY-based efficiencies, reflecting the performance of impurity-containing samples, are inferior to those derived from considering only excitonic effects. This implies that there is still room for improving the TMDC samples to attain greater PCEs.

The obtained efficiencies can be compared with previous theoretical studies. For instance, Ozdemir and Baroni⁶¹ investigated the photovoltaic efficiency of bulk TMDCs based on ab initio many-body perturbation theory calculations, including the e-h interaction. In their work, the absorptivity is calculated as $A = 1 - T - R$, where T is the transmittivity and R is the reflectivity, and those properties are computed from Fresnel's equations. For TMDCs with a thickness of 10^3 nm, the same ones analyzed in our work, they reported values of PCE in a range of $\sim 21\%$ to $\sim 26\%$, being the selenides the most efficient systems, consistent with our findings, especially those that account for nonradiative recombination through PLQY experiments.

Furthermore, Chouldhary et al.⁶² have reported theoretical results of SLME based on DFT without taking e-h interactions into account. The η_{SLME} computed for a thickness of 500 nm were 18.6%, 27.6%, 15.2%, and 21.5% for bulk MoS₂, MoSe₂, WS₂, and WSe₂, respectively. Although in that work the authors have used band gaps calculated at the DFT level with meta-GGA functionals, their SLME efficiencies lie between our predicted values modeled by the SLME-X and SLME-PLQY approaches.

Finally, despite the large range of efficiencies, we verify that the selenides present higher efficiencies, with MoSe₂ and WSe₂ photovoltaic efficiencies being almost the same. Our results highlight the importance of the fraction of radiative e-h recombination factor (f_r) to determine the maximum PCEs of bulk TMDCs, which indeed can be extrapolated to other indirect band gap absorbers. In particular, we present a range of values for this relevant solar cell parameter and their corresponding efficiencies, based on several approaches that can represent reliable upper limits for the photovoltaic efficiencies of single-junction solar devices produced with TMDC thin films.

Conclusions

We carried out first-principles calculations based on DFT combined with many-body perturbation theory within the G_0W_0 -BSE framework to study the optical response and the photovoltaic properties of bulk 2H-MX₂ (M = Mo, W, and X = S, Se), using for the latter the spectroscopic limited maximum efficiency (SLME) formalism. Our results indicated that an accurate description of the optical spectrum within the GW -BSE framework requires mapping out the Brillouin zone in very fine k -grid samples. The agreement obtained when comparing the BSE optical spectra and the experimental ones highlights the excitons' roles in the optical absorption of bulk TMDCs. The calculated power conversion efficiencies (PCEs) of the analyzed TMDCs were overestimated with the Shockley-Queisser formalism, as expected since in this approach one includes only radiative e-h recombination losses. On the other hand, the standard SLME approach tends to underestimate the PCE of these van der Waals materials, due to a quite small estimate of the fraction of radiative recombination. In other words, for the standard SLME, almost all the recombination processes should correspond to nonradiative losses. These findings have motivated us to explore alternative methods for modeling PCEs that account for radiative and nonradiative recombination processes in more realistic ways. Thus, we investigate the modeling of the fraction of e-h recombination processes by considering the energy range from exciton eigenvalues (SLME-X), and also by employing experimental results obtained for photoluminescence quantum yield (SLME-PLQY). As a result, we predict that when we adopt the exciton energy ranges to compute the PCE within the SLME-X approach, the maximum PCEs vary between $\sim 23 - 29\%$, whereas taking the experimental fraction of radiative e-h recombination from PLQY experiments within the SLME-PLQY approach, the bulk TMDC maximum PCEs reached values between $\sim 19 - 24\%$. Regardless of the approach used to determine the PCE, our results indicate that the selenide-based TMDCs exhibit superior photovoltaic efficiency in comparison to the sulfide-based ones. In conclusion, we believe that our comprehensive analysis of the effects of the fraction of e-h radiative recombination in the TMDC efficiencies

can be used as accurate predictions of upper limits for the photovoltaic efficiencies of solar devices based on few-layer or multi-layer TMDCs, paving the way for the development of efficient nanoscopically thin solar cells.

Acknowledgements

E.M.Jr and A.R.R. acknowledge the financial support from the Brazilian agency FAPESP, Grant No. 20/13172-8 and 2017/02317-2. This research was supported by resources supplied by CENAPAD-SP and the Center for Scientific Computing (NCC/GridUNESP) of the UNESP.

References

- (1) Han, X. Ductile van der Waals materials. *Science* **2020**, *369*, 509–509.
- (2) Novoselov, K. S.; Geim, A. K.; Morozov, S. V.; Jiang, D.; Zhang, Y.; Dubonos, S. V.; Grigorieva, I. V.; Firsov, A. A. Electric Field Effect in Atomically Thin Carbon Films. *Science* **2004**, *306*, 666–669.
- (3) Khan, K.; Tareen, A. K.; Aslam, M.; Wang, R.; Zhang, Y.; Mahmood, A.; Ouyang, Z.; Zhang, H.; Guo, Z. Recent developments in emerging two-dimensional materials and their applications. *J. Mater. Chem. C* **2020**, *8*, 387–440.
- (4) Ma, Q.; Ren, G.; Xu, K.; Ou, J. Z. Tunable optical properties of 2D materials and their applications. *Adv. Opt. Mater.* **2021**, *9*, 2001313.
- (5) Villegas, C. E. P.; Rocha, A. R. Near-Infrared Optical Response and Carrier Dynamics for High Photoconversion in Tellurene. *J. Phys. Chem. C* **2022**, *126*, 6129–6134.
- (6) Chhowalla, M.; Shin, H. S.; Eda, G.; Li, L.-J.; Loh, K. P.; Zhang, H. The chemistry of

- two-dimensional layered transition metal dichalcogenide nanosheets. *Nat. Chem.* **2013**, *5*, 263–275.
- (7) Manzeli, S.; Ovchinnikov, D.; Pasquier, D.; Yazyev, O. V.; Kis, A. 2D transition metal dichalcogenides. *Nat. Rev. Mater.* **2017**, *2*, 17033–15.
- (8) Perez, A.; Amorim, R. G.; Villegas, C. E. P.; Rocha, A. R. Nanogap-based all-electronic DNA sequencing devices using MoS₂ monolayers. *Phys. Chem. Chem. Phys.* **2020**, *22*, 27053–27059.
- (9) Villegas, C. E. P.; Rocha, A. R. Elucidating the optical properties of novel heterolayered materials based on MoTe₂–InN for photovoltaic applications. *J. Phys. Chem. C* **2015**, *119*, 11886–11895.
- (10) Britnell, L.; Ribeiro, R. M.; Eckmann, A.; Jalil, R.; Belle, B. D.; Mishchenko, A.; Kim, Y.-J.; Gorbachev, R. V.; Georgiou, T.; Morozov, S. V.; Grigorenko, A. N.; Geim, A. K.; Casiraghi, C.; Neto, A. H. C.; Novoselov, K. S. Strong Light-Matter Interactions in Heterostructures of Atomically Thin Films. *Science* **2013**, *340*, 1311–1314.
- (11) Furchi, M. M.; Höller, F.; Dobusch, L.; Polyushkin, D. K.; Schuler, S.; Mueller, T. Device physics of van der Waals heterojunction solar cells. *npj 2D Mater. Appl.* **2018**, *2*, 3.
- (12) Baugher, B. W.; Churchill, H. O.; Yang, Y.; Jarillo-Herrero, P. Optoelectronic devices based on electrically tunable p–n diodes in a monolayer dichalcogenide. *Nat. Nanotechnol.* **2014**, *9*, 262–267.
- (13) Kim, H. G.; Choi, H. J. Thickness dependence of work function, ionization energy, and electron affinity of Mo and W dichalcogenides from DFT and GW calculations. *Phys. Rev. B* **2021**, *103*, 1–9.

- (14) Aftab, S.; Iqbal, M. Z.; Hussain, S.; Hegazy, H. H.; Saeed, M. A. Transition metal dichalcogenides solar cells and integration with perovskites. *Nano Energy* **2023**, *108*, 108249.
- (15) Nassiri Nazif, K.; Kumar, A.; Hong, J.; Lee, N.; Islam, R.; McClellan, C. J.; Karni, O.; van de Groep, J.; Heinz, T. F.; Pop, E.; Brongersma, M. L.; Saraswat, K. C. High-performance p–n junction transition metal dichalcogenide photovoltaic cells enabled by MoO_x doping and passivation. *Nano Lett.* **2021**, *21*, 3443–3450.
- (16) He, X.; Iwamoto, Y.; Kaneko, T.; Kato, T. Fabrication of near-invisible solar cell with monolayer WS₂. *Sci. Rep.* **2022**, *12*, 11315.
- (17) Bernardi, M.; Palummo, M.; Grossman, J. C. Extraordinary Sunlight Absorption and One Nanometer Thick Photovoltaics Using Two-Dimensional Monolayer Materials. *Nano Lett.* **2013**, *13*, 3664–3670.
- (18) Britnell, L.; Ribeiro, R. M.; Eckmann, A.; Jalil, R.; Belle, B. D.; Mishchenko, A.; Kim, Y.-J.; Gorbachev, R. V.; Georgiou, T.; Morozov, S. V.; Grigorenko, A. N.; Geim, A. K.; Casiraghi, C.; Neto, A. H. C.; Novoselov, K. S. Strong light-matter interactions in heterostructures of atomically thin films. *Science* **2013**, *340*, 1311–1314.
- (19) Li, H.-M.; Lee, D.; Qu, D.; Liu, X.; Ryu, J.; Seabaugh, A.; Yoo, W. J. Ultimate thin vertical p–n junction composed of two-dimensional layered molybdenum disulfide. *Nat. Comm.* **2015**, *6*, 6564.
- (20) Cheng, R.; Li, D.; Zhou, H.; Wang, C.; Yin, A.; Jiang, S.; Liu, Y.; Chen, Y.; Huang, Y.; Duan, X. Electroluminescence and Photocurrent Generation from Atomically Sharp WSe₂/MoS₂ Heterojunction p–n Diodes. *Nano Lett.* **2014**, *14*, 5590–5597.
- (21) Mao, X.; Zou, J.; Li, H.; Song, Z.; He, S. Magnetron sputtering fabrication and photoelectric properties of WSe₂ film solar cell device. *Appl. Surf. Sci.* **2018**, *444*, 126–132.

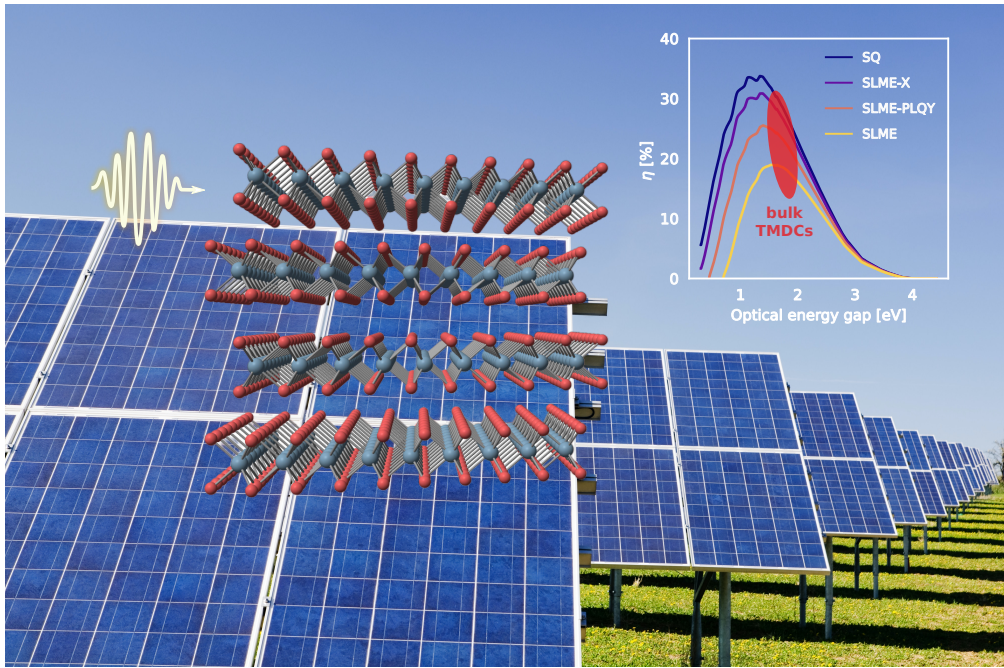
- (22) Went, C. M.; Wong, J.; Jahelka, P. R.; Kelzenberg, M.; Biswas, S.; Hunt, M. S.; Carbone, A.; Atwater, H. A. A new metal transfer process for van der Waals contacts to vertical Schottky-junction transition metal dichalcogenide photovoltaics. *Sci. Adv.* **2019**, *5*, eaax6061.
- (23) McVay, E.; Zubair, A.; Lin, Y.; Nourbakhsh, A.; Palacios, T. Impact of Al₂O₃ passivation on the photovoltaic performance of vertical WSe₂ Schottky junction solar cells. *ACS Appl. Mater. Interfaces* **2020**, *12*, 57987–57995.
- (24) Islam, K. M.; Ismael, T.; Luthy, C.; Kizilkaya, O.; Escarra, M. D. Large-Area, High-Specific-Power Schottky-Junction Photovoltaics from CVD-Grown Monolayer MoS₂. *ACS Applied Materials & Interfaces* **2022**, *14*, 24281–24289.
- (25) Liu, Y.; Guo, J.; Zhu, E.; Liao, L.; Lee, S.-J.; Ding, M.; Shakir, I.; Gambin, V.; Huang, Y.; Duan, X. Approaching the Schottky–Mott limit in van der Waals metal–semiconductor junctions. *Nature* **2018**, *557*, 696–700.
- (26) Lee, C.-H.; Lee, G.-H.; van der Zande, A. M.; Chen, W.; Li, Y.; Han, M.; Cui, X.; Arefe, G.; Nuckolls, C.; Heinz, T. F.; Guo, J.; Hone, J.; Kim, P. Atomically thin p–n junctions with van der Waals heterointerfaces. *Nat. Nanotechnol.* **2014**, *9*, 676–681.
- (27) Memaran, S.; Pradhan, N. R.; Lu, Z.; Rhodes, D.; Ludwig, J.; Zhou, Q.; Ogunsolu, O.; Ajayan, P. M.; Smirnov, D.; Fernández-Domínguez, A. I.; García-Vidal, F. J.; Balicas, L. Pronounced photovoltaic response from multilayered transition-metal dichalcogenides PN-junctions. *Nano Lett.* **2015**, *15*, 7532–7538.
- (28) Cho, A.-J.; Song, M.-K.; Kang, D.-W.; Kwon, J.-Y. Two-Dimensional WSe₂/MoS₂ p–n Heterojunction-Based Transparent Photovoltaic Cell and Its Performance Enhancement by Fluoropolymer Passivation. *ACS Appl. Mater. Interfaces* **2018**, *10*, 35972–35977.
- (29) Nassiri Nazif, K.; Daus, A.; Hong, J.; Lee, N.; Vaziri, S.; Kumar, A.; Nitta, F.; Chen, M. E.; Kananian, S.; Islam, R.; Kim, K.-H.; Park, J.-H.; Poon, A. S. Y.;

- Brongersma, M. L.; Pop, E.; Saraswat, K. C. High-specific-power flexible transition metal dichalcogenide solar cells. *Nat. Commun.* **2021**, *12*, 7034.
- (30) Ozório, M. S.; Dias, A. C.; Silveira, J. F.; Da Silva, J. L. Theoretical Investigation of the Role of Anion and Trivalent Cation Substitution in the Physical Properties of Lead-Free Zero-Dimensional Perovskites. *J. Phys. Chem. C* **2022**, *126*, 7245–7255.
- (31) Hohenberg, P.; Kohn, W. Inhomogeneous electron gas. *Phys. Rev.* **1964**, *136*, B864.
- (32) Kohn, W.; Sham, L. J. Self-consistent equations including exchange and correlation effects. *Phys. Rev.* **1965**, *140*, A1133.
- (33) Giannozzi, P.; Baroni, S.; Bonini, N.; Calandra, M.; Car, R.; Cavazzoni, C.; Ceresoli, D.; Chiarotti, G. L.; Cococcioni, M.; Dabo, I.; Corso, A. D.; de Gironcoli, S.; Fabris, S.; Fratesi, G.; Gebauer, R.; Gerstmann, U.; Gougoussis, C.; Kokalj, A.; Lazzeri, M.; Martin-Samos, L.; Marzari, N.; Mauri, F.; Mazzarello, R.; Paolini, S.; Pasquarello, A.; Paulatto, L.; Sbraccia, C.; Scandolo, S.; Sclauzero, G.; Seitsonen, A. P.; Smogunov, A.; Umari, P.; Wentzcovitch, R. M. QUANTUM ESPRESSO: a modular and open-source software project for quantum simulations of materials. *J. Phys.: Condens. Matter* **2009**, *21*, 395502.
- (34) Perdew, J. P.; Burke, K.; Ernzerhof, M. Generalized gradient approximation made simple. *Phys. Rev. Lett.* **1996**, *77*, 3865.
- (35) Hamann, D. R. Optimized norm-conserving Vanderbilt pseudopotentials. *Phys. Rev. B* **2013**, *88*, 085117.
- (36) Grimme, S. Semiempirical GGA-type density functional constructed with a long-range dispersion correction. *J. Comput. Chem.* **2006**, *27*, 1787–1799.
- (37) Hedin, L. New Method for Calculating the One-Particle Green’s Function with Application to the Electron-Gas Problem. *Phys. Rev.* **1965**, *139*, A796–A823.

- (38) Marini, A.; Hogan, C.; Grüning, M.; Varsano, D. yambo: An ab initio tool for excited state calculations. *Comput. Phys. Commun.* **2009**, *180*, 1392–1403.
- (39) Bruneval, F.; Gonze, X. Accurate *GW* self-energies in a plane-wave basis using only a few empty states: Towards large systems. *Phys. Rev. B* **2008**, *78*, 085125.
- (40) Rohlfing, M.; Louie, S. G. Electron-hole excitations and optical spectra from first principles. *Phys. Rev. B* **2000**, *62*, 4927–4944.
- (41) Kammerlander, D.; Botti, S.; Marques, M. A.; Marini, A.; Attaccalite, C. Speeding up the solution of the Bethe-Salpeter equation by a double-grid method and Wannier interpolation. *Phys. Rev. B* **2012**, *86*, 125203.
- (42) Supporting information: convergence analyses of *GW* and BSE calculations, and results of photovoltaic properties of the bulk TMDCs within Shockley-Queisser formalism.
- (43) Wildervanck, J.; Jellinek, F. Preparation and crystallinity of molybdenum and tungsten sulfides. *Z. Anorg. Allg. Chem.* **1964**, *328*, 309.
- (44) Schutte, W.; De Boer, J.; Jellinek, F. Crystal structures of tungsten disulfide and diselenide. *J. Solid State Chem.* **1987**, *70*, 207–209.
- (45) Evans, B.; Hazelwood, R. Optical and structural properties of MoSe₂. *Phys. Status Solidi (A)* **1971**, *4*, 181.
- (46) Kim, B. S.; Rhim, J.-W.; Kim, B.; Kim, C.; Park, S. R. Determination of the band parameters of bulk 2H-MX₂ (M= Mo, W; X= S, Se) by angle-resolved photoemission spectroscopy. *Sci. Rep.* **2016**, *6*, 36389.
- (47) Beal, A.; Liang, W.; Hughes, H. Kramers-Kronig analysis of the reflectivity spectra of 3R-WS₂ and 2H-WSe₂. *J. Phys. C: Solid State Phys.* **1976**, *9*, 2449.
- (48) Beal, A.; Hughes, H. Kramers-Kronig analysis of the reflectivity spectra of 2H-MoS₂, 2H-MoSe₂ and 2H-MoTe₂. *J. Phys. C: Solid State Phys.* **1979**, *12*, 881.

- (49) Li, Y.; Chernikov, A.; Zhang, X.; Rigosi, A.; Hill, H. M.; Van Der Zande, A. M.; Chenet, D. A.; Shih, E.-M.; Hone, J.; Heinz, T. F. Measurement of the optical dielectric function of monolayer transition-metal dichalcogenides: MoS₂, MoSe₂, WS₂, and WSe₂. *Phys. Rev. B* **2014**, *90*, 205422.
- (50) Wang, G.; Chernikov, A.; Glazov, M. M.; Heinz, T. F.; Marie, X.; Amand, T.; Urbaszek, B. Colloquium: Excitons in atomically thin transition metal dichalcogenides. *Rev. Mod. Phys.* **2018**, *90*, 021001.
- (51) Yu, L.; Zunger, A. Identification of Potential Photovoltaic Absorbers Based on First-Principles Spectroscopic Screening of Materials. *Phys. Rev. Lett.* **2012**, *108*, 068701.
- (52) Shockley, W.; Queisser, H. J. Detailed Balance Limit of Efficiency of p-n Junction Solar Cells. *J. Appl. Phys.* **1961**, *32*, 510–519.
- (53) Mohamed, N. B.; Lim, H. E.; Wang, F.; Koirala, S.; Mouri, S.; Shinokita, K.; Miyauchi, Y.; Matsuda, K. Long radiative lifetimes of excitons in monolayer transition-metal dichalcogenides MX₂ (M= Mo, W; X= S, Se). *Appl. Phys. Express* **2017**, *11*, 015201.
- (54) Bercx, M.; Sarmadian, N.; Saniz, R.; Partoens, B.; Lamoen, D. First-principles analysis of the spectroscopic limited maximum efficiency of photovoltaic absorber layers for CuAu-like chalcogenides and silicon. *Phys. Chem. Chem. Phys.* **2016**, *18*, 20542–20549.
- (55) Moujaes, E. A.; Dias, A. C. On the excitonic effects of the 1T and 1OT phases of PdS₂, PdSe₂, and PdSSe monolayers. *J. Phys. Chem. Solids* **2023**, *182*, 111573.
- (56) Dreessen, C.; Zanoni, K. P. S.; Gil-Escrig, L.; Rodkey, N.; Khan, J. I.; Laquai, F.; Sessolo, M.; Roldán-Carmona, C.; Bolink, H. J. When JV Curves Conceal Material Improvements: The Relevance of Photoluminescence Measurements in the Optimization of Perovskite Solar Cells. *Adv. Opt. Mater.* **2023**, *n/a*, 2301019.

- (57) Jariwala, D.; Davoyan, A. R.; Wong, J.; Atwater, H. A. Van der Waals materials for atomically-thin photovoltaics: promise and outlook. *ACS Photonics* **2017**, *4*, 2962–2970.
- (58) Amani, M.; Lien, D.-H.; Kiriya, D.; Xiao, J.; Azcatl, A.; Noh, J.; Madhvapathy, S. R.; Addou, R.; KC, S.; Dubey, M.; Cho, K.; Wallace, R. M.; Lee, S.-C.; He, J.-H.; Ager, J. W.; Zhang, X.; Yablonovitch, E.; Javey, A. Near-unity photoluminescence quantum yield in MoS₂. *Science* **2015**, *350*, 1065–1068.
- (59) Amani, M.; Taheri, P.; Addou, R.; Ahn, G. H.; Kiriya, D.; Lien, D.-H.; Ager III, J. W.; Wallace, R. M.; Javey, A. Recombination kinetics and effects of superacid treatment in sulfur-and selenium-based transition metal dichalcogenides. *Nano Lett.* **2016**, *16*, 2786–2791.
- (60) Mak, K. F.; Lee, C.; Hone, J.; Shan, J.; Heinz, T. F. Atomically thin MoS₂: a new direct-gap semiconductor. *Phys. Rev. Lett.* **2010**, *105*, 136805.
- (61) Ozdemir, B.; Barone, V. Thickness dependence of solar cell efficiency in transition metal dichalcogenides MX₂ (M: Mo, W; X: S, Se, Te). *Sol. Energy Mater. Sol. Cells* **2020**, *212*, 110557.
- (62) Choudhary, K.; Bercx, M.; Jiang, J.; Pachter, R.; Lamoen, D.; Tavazza, F. Accelerated discovery of efficient solar cell materials using quantum and machine-learning methods. *Chem. Mater.* **2019**, *31*, 5900–5908.



TOC Graphic